European Journal of Wood and Wood Products manuscript No.
(will be inserted by the editor)

Predicting Layer Cracks in Cross-Laminated Timber with Evaluations of Strategies for Suppressing Them

John A. Nairn

Accepted: March 3, 2019

Abstract Cross Laminated Timber (CLT) is made by laminating three or more timber layers with grain directions in alternate layers at right angles to each other. This structure, with its numerous wood bonds glued in cross-grained directions, develops residual stresses whenever panels are exposed to variations in temperature or moisture content. This paper analyzes how these residual stresses combined with mechanical stresses can cause CLT cracks by deriving an expression for energy released when a new crack forms within one layer. By using finite fracture mechanics concepts, where a crack forms when energy released by that crack exceeds the transverse toughness of wood, this equation can predict layer cracking under many conditions. Two specific examples given are cracking due to residual shrinkage alone and cracking due to uniaxial tension. Finite fracture mechanics and energy release calculations provide useful tools for designing durable CLT products and structures. Various options for improving CLT are considered along with needs for more analysis and experiments. Two simple changes to CLT that could greatly enhance durability are to use thinner layers and to sufficiently dry the timber before panel fabrication.

Keywords Cross Laminated Timber · Layer Cracks · Delamination · Fracture Mechanics

1 Introduction

Woodworkers have known for centuries that one must never glue wood in cross-grained directions because such joints are likely to crack. If a crossed-grain connection is needed, it is screwed instead of glued and the screws require slots to accommodate wood movement. Solid wood tops must be attached to a base with table fasteners that accommodate shrinkage or expansion of the top. Frame and panel doors are used to avoid cross-grained gluing. Solid wood panels float (without glue) within a frame of straight-grained stiles. Nevertheless, several engineered wood products go against this acquired wisdom. One recent example is cross laminated timber (CLT) that is made by laminating three or more timber layers with grain directions in alternate layers at right angles to each other. The timber faces between layers are glued resulting in cross-grained bonds. Can such a structure avoid cracks? The short answer is that modest levels of mechanical and residual stresses will cause CLT to crack. Mechanical stresses arise from loads on structures and are unavoidable. Residual stresses are caused by exposure to variations in temperature and humidity that result in differential shrinkage or expansion between layers. Any net shrinkage that occurs causes transverse tensile residual stresses that promote layer cracking.

The causes of CLT cracking can be modeled by assuming a crack spanning one layer forms when energy released by formation of that crack reaches the toughness of the wood layer. This concept is known as finite fracture mechanics (Hashin, 1996; Nairn, 1999). It extends conventional fracture mechanics, which predicts propagation of a single, dominant crack, to failure predictions in materials that progressively fail by fracture events. CLT layer cracking is one example of fracture events. Other examples include microcracking of cross-ply, aerospace composites (Parvizi

John A. Nairn
Oregon State University, Wood Science & Engineering
112 Richardson Hall, Corvallis, OR 97330, USA
Tel.: +1-541-737-4265, Fax: +1-541-737-3385, E-mail: John.Nairn@oregonstate.edu

et al, 1978; Nairn and Hu, 1994; Nairn, 2000), cracking of paints (Kim and Nairn, 2000a,b; Nairn and Kim, 1992) and coatings (Leterrier et al, 2009, 2003, 1997b,a), mud cracks in deserts (Groisman and Kaplan, 1994), cavitation of rubber (Gent and Wang, 1991; Gent, 1990; Gent and Lindley, 1959), and internal ring checking in wood (Pang et al, 1999; Nairn, 2010). The ability of finite fracture mechanics to predict layer cracking has been confirmed by experiments (Nairn et al, 1993; Nairn and Hu, 1994; Nairn, 2000) and theoretical arguments (McCartney, 2008).

Why should CLT be singled out as sensitive to residual stresses and cracking while solid wood and other mass-timber products, such as glulam, are not? The reason is that solid wood and glulam both have wood grain in a single direction. As a result, they experience lower residual stresses. Cracks that form are usually of limited depth and aligned in one direction. In contrast, CLT's cross-grained structure causes higher residual stress. Cracks develop more easily, develop throughout the panel, and occur in two directions. Why should CLT be singled out when compared to other engineered wood products with cross-grained bonds such as plywood or oriented strand board? The reason is that failure has scaling effects. In layer cracking, the scaling is with layer thickness (Nairn, 2000) implying that durability decreases as layers get thicker. For example, a CLT panel with 38.1 mm (1.5 in.) dimensioned timber compared to plywood with 1.58 mm (1/16 in.) veneers would have $38.1/1.58 = 24$ times the energy available to cause cracking. CLT is sometimes referred to as "plywood on steroids." If this analogy is similar to "athletes on steroids," who get a short-term boost at the cost of life-threatening consequences later, then it may be an appropriate moniker for CLT.

This paper finds an exact expression for energy released by formation of layer cracks in a CLT panel under in-plane mechanical loads along with residual stresses caused by changes in temperature or moisture content. The derived general expression is exact, but is expressed in terms of effective panel mechanical properties. By using variational mechanics models for mechanical properties of cracked CLT (Hashin, 1987; Nairn, 2017), explicit results were derived for analyzing many CLT cracking situations. They were used to predict cracks caused by moisture shrinkage alone or by uniaxial tensile loading. The new finite fracture mechanics equations provide useful tools for understanding CLT, predicting its durability, and designing improved CLT products. The discussion section considers strategies for suppressing cracks, durability analysis methods, and delamination failure. This paper concludes with recommendations for more analysis and key experiments.

2 Finite Fracture Mechanics of a CLT Panel with Residual Stresses

This section finds energy release rate due to formation of a layer crack caused by in-plane mechanical and residual stresses. Figure 1 shows a unit cell for a three-layer CLT panel with transverse cracks in all layers (Hashin, 1987). The core layer (labeled 1) has thickness $2t_1$, cracks at $x = \pm a$, and wood grain at 90° to the 1 direction. The surface layers (labeled 2) have thickness t_2, cracks at $y = \pm b$, and wood grain at 0° to the 1 direction. This unit cell describes a panel with crack densities $D_a = 1/(2a)$ and $D_b = 1/(2b)$ in the two layers. In typical "as-made" CLT, $t_2 = 2t_1$ is thickness and $2a = 2b$ is width of the panel's timber. Because timber edges are usually not glued, those edges act as precracks. When additional cracks form, a and b decrease. Various other terms used here are collected in Table 1.

If the crack spacings on the panel's 1-3 surface are all equal to $2a$ and on the 2-3 surface are all equal to $2b$, the unit cell would be a repeating unit and all unit cells would have the same stress state. This condition is approximately true in "as-made" CLT with constant-width timbers. But, importantly, this analysis *does not require* a repeating unit cell. As explained by Hashin (1987), a rigorous, complementary energy analysis permits variable size unit cells with the full laminate being a statistical average of crack spacings. In other words a and b will be random variables describing distributions of crack spacing on the panel's 1-3 and 2-3 surfaces. The analysis does assume, however, that cracks on each surface extend through the layer to the opposite side of the laminate (see Fig. 1 in Hashin (1987)). Such an analysis can predict formation of complete layers cracks but does model propagation phase of cracks prior to becoming complete cracks. Experimental observations of layer cracking consistently show that once a crack initiates it rapidly (often unstably) forms a complete crack in the layer (Nairn and Hu, 1994; Nairn, 2000; McCartney, 2008).

The energy release rate due to any increment in fracture area, dA, within a composite with residual thermal stresses is derived in Nairn (1997):

$$G = G_{mech} + \frac{V}{2}\left(2\frac{d\langle\boldsymbol{\sigma}^m\cdot\boldsymbol{\alpha}\Delta T\rangle}{dA} + \frac{d\langle\boldsymbol{\sigma}^r\cdot\boldsymbol{\alpha}\Delta T\rangle}{dA}\right) \tag{1}$$

where V is total volume, total stress is partitioned as $\boldsymbol{\sigma} = \boldsymbol{\sigma}^m + \boldsymbol{\sigma}^r$, and angle brackets indicates a volume-averaged quantity. This section uses Eq. (1) to derive an exact result for G due to formation of layer cracks in CLT caused by normal stresses σ_{10} and σ_{20} in the 1 and 2 directions and residual stresses. For simplicity, the derivation considers

Table 1 Nomenclature for various terms used throughout this paper. The functional dependence (a,b) refers to a CLT panel property when crack spacings are a and b in core and surface layers respectively. CTE and CME refer to coefficients of thermal and moisture expansion.

Term	Definition	Term	Definition
G	Energy release rate	G_{mech}	Mechanical energy release rate
σ, σ^m, σ^r	total, mechanical and residual stress	$\sigma_{ij}^{(k)}$, $\sigma_{ij}^{(km)}$, $\sigma_{ij}^{(kr)}$	Stress in layer k with $i = x,y,z$
α, $\alpha^{(k)}$, $\alpha_{ii}^{(k)}$	Layer k CTE $i = x,y,z$	ΔT	Temperature change inducing residual stresses
$\beta_{ii}^{(k)}$	Layer k CME $i = x,y,z$	Δc	Moisture change inducing residual stresses
σ_{10}, σ_{20}	Applied panel stress in direction 1 or 2	$E_{ii}(a,b)$	Panel modulus in direction $i = 1,2$
$\nu_{ij}(a,b)$	Panel Poison's ratio in direction $i,j = 1,2$	$\alpha_{ii}(a,b)$	Panel CTE in direction $i = 1,2$
$E_{ii}^{(k)}$, $G_{ij}^{(k)}$	Layer k tensile and shear moduli $i,j = x,y$	$\nu_{ij}^{(k)}$	Layer k Poisson's ratio $i = x,y,z$

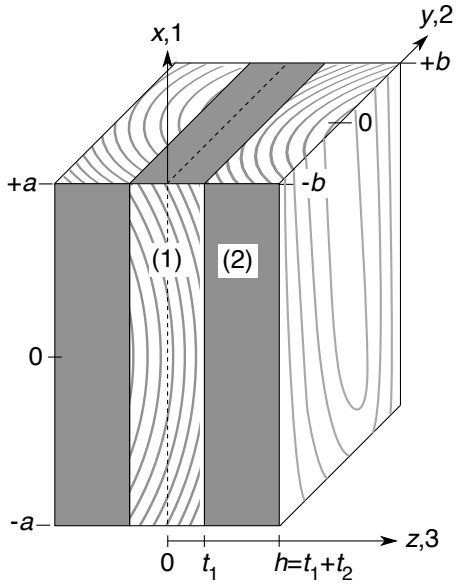

Fig. 1 Unit cell for a CLT panel with orthogonal cracking in all layers. The gray planes mark the crack surfaces (one on each end of each layer) with normals perpendicular to wood grain direction in each layer. Layer 1 is core layer with thickness $2t_1$ and cracks separated by $2a$. Layers 2 are surface layers with thickness t_2 and cracks separated by $2b$. Axes $(1,2,3)$ are used to refer to panel properties while (x,y,z) refer to layer properties.

only residual thermal stresses, but the final form accounts for a combination of thermal and moisture induced residual stress. For brevity, this derivation omits some details. More details are available in this paper's *Online Resource*.

The mechanical energy release rate for a composite under traction loads $\mathbf{T}_0$ applied on surface S_T is (Nairn, 1997):

$$G_{mech} = \frac{1}{2}\frac{d}{dA}\int_{S_T} \mathbf{T}^0 \cdot \mathbf{u}^m dS \tag{2}$$

where $\mathbf{u}_m$ is surface displacement due to mechanical stresses. G_{mech} can be evaluated by treating S_T as the uncracked surfaces with loads $\pm h\sigma_{10}/t_2$ and displacements $\pm a\varepsilon_{10}^m$ on top and bottom of layer 2 and loads $\pm h\sigma_{20}/t_1$ and displacements $\pm b\varepsilon_{20}^m$ on sides of layer 1. Evaluating the surface integrals and expressing global strains in terms of effective panel properties (*e.g.*, $\varepsilon_{10}^m = \sigma_{10}/E_{11}(a,b) - \nu_{12}\sigma_{20}/E_{11}(a,b)$), G_{mech} evaluates to

$$G_{mech} = \frac{V}{2}\frac{d}{dA}\left(\frac{\sigma_{10}^2}{E_{11}(a,b)} - \frac{2\nu_{12}(a,b)\sigma_{10}\sigma_{20}}{E_{11}(a,b)} + \frac{\sigma_{20}^2}{E_{22}(a,b)}\right) \tag{3}$$

The next steps express the remaining terms in Eq. (1) using effective mechanical properties. The derivations start with the Levin (1967) equation that takes this form for CLT:

$$\sigma^m \cdot \alpha(a,b) = \sum_{k=1}^{2} V_k \overline{\sigma^{(km)}} \cdot \alpha^{(k)} \tag{4}$$

where σ^m is any applied mechanical stress, V_k is volume fraction of layer k, and an over bar indicates a quantity averaged over a phase's volume. For in-plane x-y mechanical loads, the Levin equation gives:

$$\langle \sigma^m \cdot \alpha \Delta T \rangle = \sum_{k=1}^{2} V_k \left(\overline{\sigma_{xx}^{(km)}} \alpha_{xx}^{(k)} + \overline{\sigma_{yy}^{(km)}} \alpha_{yy}^{(k)} \right) \Delta T = \sigma_{10} \alpha_{11}(a,b) \Delta T + \sigma_{20} \alpha_{22}(a,b) \Delta T \tag{5}$$

A second use of the Levin equation can eliminate the effective CTEs. First consider mechanical loading in direction 1 only. The Levin equation becomes:

$$\sigma_{10} \alpha_{11}(a,b) \Delta T = \sum_{k=1}^{2} V_k \left(\overline{\sigma_{xx}^{(km)}} \alpha_{xx}^{(k)} + \overline{\sigma_{yy}^{(km)}} \alpha_{yy}^{(k)} \right) \Delta T \tag{6}$$

where phase average stress now refer to uniaxial loading. They can be evaluated from these six global relations:

$$\begin{array}{cc} \sigma_{10} = V_1 \overline{\sigma_{xx}^{(1)}} + V_2 \overline{\sigma_{xx}^{(2)}} & 0 = V_1 \overline{\sigma_{yy}^{(1)}} + V_2 \overline{\sigma_{yy}^{(2)}} \\ \overline{\sigma_{xx}^{(1)}} = Q_{xx}^{(1)} (\overline{\varepsilon_{xx}^{(1)}} - \alpha_{xx}^{(1)} \Delta T) + Q_{xy}^{(1)} (\overline{\varepsilon_{yy}^{(1)}} - \alpha_{yy}^{(1)} \Delta T) & \overline{\sigma_{yy}^{(1)}} = Q_{xy}^{(1)} (\overline{\varepsilon_{xx}^{(1)}} - \alpha_{xx}^{(1)} \Delta T) + Q_{yy}^{(1)} (\overline{\varepsilon_{yy}^{(1)}} - \alpha_{yy}^{(1)} \Delta T) \\ \overline{\sigma_{xx}^{(2)}} = Q_{xx}^{(2)} (\overline{\varepsilon_{xx}^{(2)}} - \alpha_{xx}^{(2)} \Delta T) + Q_{xy}^{(2)} (\overline{\varepsilon_{yy}^{(2)}} - \alpha_{yy}^{(2)} \Delta T) & \overline{\sigma_{yy}^{(2)}} = Q_{xy}^{(2)} (\overline{\varepsilon_{xx}^{(2)}} - \alpha_{xx}^{(2)} \Delta T) + Q_{yy}^{(1)} (\overline{\varepsilon_{yy}^{(2)}} - \alpha_{yy}^{(2)} \Delta T) \end{array} \tag{7}$$

The first two equations are force balance in the two panel directions. The next four relate phase average stresses to phase average strains where $Q_{ij}^{(k)}$ are elements of the laminated plate theory stiffness tensor for layer k:

$$\begin{pmatrix} \sigma_{xx}^{(k)} \\ \sigma_{yy}^{(k)} \\ \sigma_{xy}^{(k)} \end{pmatrix} = \begin{pmatrix} Q_{xx}^{(k)} & Q_{xy}^{(k)} & 0 \\ Q_{xy}^{(k)} & Q_{yy}^{(k)} & 0 \\ 0 & 0 & G_{xy}^{(k)} \end{pmatrix} \begin{pmatrix} \varepsilon_{xx} - \alpha_{xx}^{(k)} \Delta T \\ \varepsilon_{yy} - \alpha_{yy}^{(k)} \Delta T \\ \gamma_{xy} \end{pmatrix}, \quad Q_{ii}^{(k)} = \frac{E_{ii}^{(k)}}{1 - \nu_{xy}^{(k)} \nu_{yx}^{(k)}}, \quad \text{and} \quad Q_{xy}^{(k)} = \frac{E_{xx}^{(k)} \nu_{yx}^{(k)}}{1 - \nu_{xy}^{(k)} \nu_{yx}^{(k)}} \tag{8}$$

These six equations have eight unknowns, but for an orthogonally-cracked CLT unit cell under mechanical loads only ($\Delta T = 0$), two average strains in the uncracked layers are equal to panel mechanical strains — $\overline{\varepsilon_{xx}^{(2m)}} = \varepsilon_{10}^m = \sigma_{10}/E_{11}(a,b)$ and $\overline{\varepsilon_{yy}^{(1m)}} = \varepsilon_{20}^m = -\nu_{12}\sigma_{10}/E_{11}(a,b)$. Solving for the remaining six unknowns and substituting stresses into Eq. (6) leads to:

$$\alpha_{11}(a,b) \Delta T = \Delta_0 - \frac{V_2 \Delta_2}{E_{11}(a,b)} + \frac{V_1 \Delta_1 \nu_{12}(a,b)}{E_{11}(a,b)} \tag{9}$$

where

$$\Delta_0 = \left(\alpha_{xx}^{(2)} + \frac{Q_{xx}^{(1)} (\alpha_{xx}^{(1)} - \alpha_{xx}^{(2)}) + Q_{xy}^{(1)} (\alpha_{yy}^{(1)} - \alpha_{yy}^{(2)})}{Q_{xx}^{(1)} Q_{yy}^{(2)} - Q_{xy}^{(1)} Q_{xy}^{(2)}} Q_{yy}^{(2)} \right) \Delta T \tag{10}$$

$$\Delta_1 = -\left(Q_{xy}^{(2)} (\alpha_{xx}^{(1)} - \alpha_{xx}^{(2)}) + Q_{yy}^{(2)} (\alpha_{yy}^{(1)} - \alpha_{yy}^{(2)}) \right) \Delta T \frac{Q_{xx}^{(1)} Q_{yy}^{(1)} - {Q_{xy}^{(1)}}^2}{Q_{xx}^{(1)} Q_{yy}^{(2)} - Q_{xy}^{(1)} Q_{xy}^{(2)}} \tag{11}$$

$$\Delta_2 = \left(Q_{xx}^{(1)} (\alpha_{xx}^{(1)} - \alpha_{xx}^{(2)}) + Q_{xy}^{(1)} (\alpha_{yy}^{(1)} - \alpha_{yy}^{(2)}) \right) \Delta T \frac{Q_{xx}^{(2)} Q_{yy}^{(2)} - {Q_{xy}^{(2)}}^2}{Q_{xx}^{(1)} Q_{yy}^{(2)} - Q_{xy}^{(1)} Q_{xy}^{(2)}} \tag{12}$$

Repeating this analysis for mechanical loading in direction 2 only leads to

$$\alpha_{22}(a,b) \Delta T = \Delta_0' - \frac{V_1 \Delta_1}{E_{22}(a,b)} + \frac{V_2 \Delta_2 \nu_{12}(a,b)}{E_{11}(a,b)} \tag{13}$$

where

$$\Delta_0' = \left(\alpha_{yy}^{(1)} + \frac{Q_{xy}^{(2)} (\alpha_{xx}^{(1)} - \alpha_{xx}^{(2)}) + Q_{yy}^{(2)} (\alpha_{yy}^{(1)} - \alpha_{yy}^{(2)})}{Q_{xx}^{(1)} Q_{yy}^{(2)} - Q_{xy}^{(1)} Q_{xy}^{(2)}} Q_{xx}^{(1)} \right) \Delta T \tag{14}$$

The Levin equation is not used for the $\langle \sigma^r \cdot \alpha \Delta T \rangle$ term because residual stresses occur when $\sigma^m = 0$. We can, however, still express that term using:

$$\langle \sigma^r \cdot \alpha \Delta T \rangle = \sum_{k=1}^{2} V_k \left(\overline{\sigma_{xx}^{(kr)}} \alpha_{xx}^{(k)} + \overline{\sigma_{yy}^{(kr)}} \alpha_{yy}^{(k)} \right) \Delta T \tag{15}$$

The phase average residual stresses are found by solving Eq. (7) with $\sigma_{10} = 0$, $\Delta T \neq 0$, and two average strains in the uncracked layers now equal to panel residual strains — $\overline{\varepsilon_{xx}^{(2r)}} = \alpha_{11}(a,b)\Delta T$ and $\overline{\varepsilon_{yy}^{(1r)}} = \alpha_{22}(a,b)\Delta T$. Solving for the remaining six unknowns and substituting stresses into Eq. (15) results in

$$\langle \sigma^r \cdot \alpha \Delta T \rangle = V_1 \Delta_1 \left(\alpha_{yy}^{(1)} - \alpha_{22}(a,b)\right)\Delta T + V_2 \Delta_2 \left(\alpha_{xx}^{(2)} - \alpha_{11}(a,b)\right)\Delta T \tag{16}$$

Substituting Eqs. (3), (5) and (16) into Eq. (1) and eliminating effective panel CTEs using Eqs. (9) and (13) gives an exact expression for energy release rate for cracking in a CLT panel under combined in-plane mechanical loads and residual thermal stresses:

$$G = \frac{V}{2}\frac{d}{dA}\left[\sigma_1^{*2}\frac{1}{E_{11}(a,b)} - 2\sigma_1^*\sigma_2^*\frac{\nu_{12}(a,b)}{E_{11}(a,b)} + \sigma_2^{*2}\frac{1}{E_{22}(a,b)}\right] \tag{17}$$

where $\sigma_1^* = \sigma_{10} - V_2\Delta_2$ and $\sigma_2^* = \sigma_{20} - V_1\Delta_1$ are two effective stresses. One more simplification is possible. For cracking only in layer 1 where a changes but b remains constant, total G must scale with a *sum* of mechanical and residual stresses (Nairn, 1997). As a consequence, one can derive an exact relation between derivatives of effective panel properties as (McCartney, 1993):

$$\frac{\left(\frac{d}{dA}\frac{\nu_{12}(a,b)}{E_{11}(a,b)}\right)_b}{\left(\frac{d}{dA}\frac{1}{E_{11}(a,b)}\right)_b} = \frac{\left(\frac{d}{dA}\frac{1}{E_{22}(a,b)}\right)_b}{\left(\frac{d}{dA}\frac{\nu_{12}(a,b)}{E_{11}(a,b)}\right)_b} \tag{18}$$

An analogous expression holds when a is held constant. Substitution into Eq. (17) leads to

$$G = \frac{V\sigma_0^{*2}}{2}\frac{d}{dA}\left[\frac{\xi}{\sqrt{E_{11}(a,b)}} + \frac{1-\xi}{\sqrt{E_{22}(a,b)}}\right]^2 \tag{19}$$

where $\sigma_0^* = \sigma_1^* + \sigma_2^*$ and $\xi = \sigma_1^*/\sigma_0^*$. Although these derivations considered only residual thermal stresses, the results are trivially extended to combine thermal and moisture residual stresses by replacing all instances of $\alpha_{ii}^{(k)}\Delta T$ with $\alpha_{ii}^{(k)}\Delta T + \beta_{ii}^{(k)}\Delta c$. Some further remarks are:

1. The energy release rate in Eq. (19) is exact, but is expressed using *effective* panel properties $E_{11}(a,b)$ and $E_{22}(a,b)$. No exact model for these properties is available, but substituting any approximate (or numerical) results gives an approximate result for G.
2. Eq. (19) specifically refers to crack formation in a unit cell with crack spacings $2a$ and $2b$. When interpreting experiments, this equation should use the crack spacings surrounding the next layer crack's location. A simple correction factor (f) is introduced below to account for panels with variable crack spacing (Nairn et al, 1993).
3. The above analysis derived G for three-layer CLT. Repeating the analysis for any number of layers, reveals it applies to CLT with any number of layers under the restriction that the unit cell can be extended in the thickness direction with all 0° layers cracked at $\pm b$ and all 90° layers cracked at $\pm a$.
4. For uniaxial loading (*e.g.*, $\sigma_{10} \neq 0$, $\sigma_{20} = 0$) with no residual stresses ($\Delta_i = 0$), this expression reduces to a standard fracture mechanics result:

$$G = \frac{V\sigma_{10}{}^2}{2}\frac{d}{dA}\left[\frac{1}{E_{11}(a,b)}\right] = \frac{P^2}{2}\frac{dC_{11}(a,b)}{dA} \tag{20}$$

where $C_{11}(a,b)$ is panel compliance in the 1 direction. Eq. (19) is significant because it extends standard fracture mechanics to include biaxial loading and, more importantly, to include residual stresses.

2.1 Explicit Calculations

Explicit energy release rate calculations need some theory or numerical results for $E_{11}(a,b)$ and $E_{22}(a,b)$. The calculations here used the 3D, variational mechanics results from Hashin (1987) and Nairn (2017) for lower-bound mechanical properties. The two tensile moduli were verified as accurate (*i.e.*, tight bounds) by comparison to 3D, numerical results. The in-plane panel moduli are:

$$\frac{1}{E_{11}(\rho_a,\rho_b)} \le \frac{1}{E_{11}^0} + \frac{V_1\chi_1(\rho_a,\rho_b)}{\rho_a\rho_b} \qquad \text{and} \qquad \frac{1}{E_{22}(\rho_a,\rho_b)} \le \frac{1}{E_{22}^0} + \frac{V_2\chi_2(\rho_a,\rho_b)}{\rho_a\rho_b} \tag{21}$$

where $\rho_a = a/t_1$ and $\rho_b = b/t_1$ are dimensionless crack spacings. E_{ii}^0 are tensile moduli for a panel with no cracks ($\rho_a = \rho_b = \infty$). These are easily found (see *Online Resource*) using laminated plate theory (Christenson, 1979). For a symmetric composite of only 0° and 90° plies, they reduce to:

$$E_{11}^0 = \langle Q_{xx}\rangle(1-\nu_{21}^0\nu_{12}^0),\ E_{22}^0 = \langle Q_{yy}\rangle(1-\nu_{21}^0\nu_{12}^0),\ \nu_{12}^0 = \frac{\langle Q_{xy}\rangle}{\langle Q_{yy}\rangle},\ \text{and}\ \nu_{21}^0 = \frac{\langle Q_{xy}\rangle}{\langle Q_{xx}\rangle} \tag{22}$$

where $\langle Q_{ij}\rangle = V_1Q_{ij}^{(1)} + V_2Q_{ij}^{(2)}$. These equations are for a single unit cell. They are used to model panel stiffness for any crack distribution by averaging (Hashin, 1987). They are used to model energy release rate by using ρ_a and ρ_b for the specific unit cell that cracks.

Because Nairn (2017) only consider panels with identical layers, those results need generalization to allow modeling panels with differing layers (such as when using different species, timber grades, or end-grain patterns (Nairn, 2007) for surface and core layers). Generalized results (see *Online Resource*) begin with new constants:

$$\begin{array}{ccc}
A_0 = \frac{1}{E_{xx}^{(1)}} + \frac{1}{\lambda E_{xx}^{(2)}} & B_0 = -\left(\frac{\nu_{yx}^{(1)}}{E_{yy}^{(1)}} + \frac{\nu_{yx}^{(2)}}{\lambda E_{yy}^{(2)}}\right) & C_0 = \frac{1}{E_{yy}^{(1)}} + \frac{1}{\lambda E_{yy}^{(2)}} \\
A_1 = \frac{1}{3G_{xz}^{(1)}} + \frac{\lambda}{3G_{xz}^{(2)}} & B_1 = \frac{1}{3G_{yz}^{(1)}} + \frac{\lambda}{3G_{yz}^{(2)}} & A_2 = \frac{(3\lambda+2)\nu_{xz}^{(1)}}{3E_{xx}^{(1)}} - \frac{\lambda\nu_{xz}^{(2)}}{3E_{xx}^{(2)}} \\
B_2 = \frac{(3\lambda+2)\nu_{yz}^{(1)}}{3E_{yy}^{(1)}} - \frac{\lambda\nu_{yz}^{(2)}}{3E_{yy}^{(2)}} & C_2 = \frac{1}{60}\left(\frac{8+20\lambda+15\lambda^2}{E_{zz}^{(1)}} + \frac{3\lambda^3}{E_{zz}^{(2)}}\right) &
\end{array} \tag{23}$$

where $\lambda = t_2/t_1$. The key functions for all calculations in this paper then become (Hashin, 1987; Nairn, 2017):

$$\frac{\chi_1(\rho_a,\rho_b)}{\rho_a\rho_b} = \frac{(1+m_{1,1})\big(\omega_1 - m_{1,1}\omega_2(1-\omega_1)\big)k_{x1}^{(1)^2}A_0 + (1+m_{1,2})\big(\omega_2 - m_{1,2}\omega_1(1-\omega_2)\big)k_{y1}^{(1)^2}C_0}{1-m_{1,1}m_{1,2}(1-\omega_1)(1-\omega_2)} \tag{24}$$

$$\frac{\chi_2(\rho_a,\rho_b)}{\lambda\rho_a\rho_b} = \frac{(1+m_{2,1})\big(\omega_1' - m_{2,1}\omega_2'(1-\omega_1')\big)k_{y2}^{(2)^2}C_0 + (1+m_{1,2})\big(\omega_2' - m_{2,2}\omega_1'(1-\omega_2')\big)k_{x2}^{(2)^2}A_0}{1-m_{2,1}m_{2,2}(1-\omega_1')(1-\omega_2')} \tag{25}$$

where $k_{xi}^{(k)}$ and $k_{yi}^{(k)}$ are influence coefficients (see Eq. (43)) and:

$$m_{1,1} = \frac{k_{y1}^{(1)}}{k_{x1}^{(1)}}\frac{B_0}{A_0},\quad m_{1,2} = \frac{k_{x1}^{(1)}}{k_{y1}^{(1)}}\frac{B_0}{C_0},\quad m_{2,1} = \frac{k_{x2}^{(2)}}{k_{y2}^{(2)}}\frac{B_0}{C_0},\quad \text{and}\quad m_{2,2} = \frac{k_{y2}^{(2)}}{k_{x2}^{(2)}}\frac{B_0}{A_0} \tag{26}$$

$$\omega_1 = \Omega\left(\rho_a, \frac{A_2-A_1}{C_2}, \frac{A_0}{C_2}\right) \quad \text{and} \quad \omega_2 = \Omega\left(\rho_b, \frac{B_2-B_1}{C_2}, \frac{C_0}{C_2}\right) \tag{27}$$

$$\omega_1' = \Omega\left(\frac{\rho_b}{\lambda}, \lambda^2\frac{B_2-B_1}{C_2}, \lambda^4\frac{C_0}{C_2}\right) \quad \text{and} \quad \omega_2' = \Omega\left(\frac{\rho_a}{\lambda}, \lambda^2\frac{A_2-A_1}{C_2}, \lambda^4\frac{A_0}{C_2}\right) \tag{28}$$

The function $\Omega(\rho,p,q)$ has two cases. When $4q > p^2$:

$$\Omega(\rho,p,q) = \frac{2\alpha\beta\big(\cosh(2\alpha\rho) - \cos(2\beta\rho)\big)}{\rho(\alpha^2+\beta^2)\big(\beta\sinh(2\alpha\rho) + \alpha\sin(2\beta\rho)\big)} \tag{29}$$

where $\alpha,\beta = \frac{1}{2}\sqrt{2\sqrt{q}\mp p}$. When $4q < p^2$:

$$\Omega(\rho,p,q) = \frac{(\alpha^2-\beta^2)\sinh(\alpha\rho)\sinh(\beta\rho)}{\rho\alpha\beta\left(\alpha\sinh(\alpha\rho)\cosh(\beta\rho)-\beta\cosh(\alpha\rho)\sinh(\beta\rho)\right)} \tag{30}$$

where $\alpha,\beta = \sqrt{-(p/2)\pm\sqrt{(p^2/4)-q}}$. Note that compared to Nairn (2017), $k_{x1}^{(1)} = k_{x1}$ and $k_{y1}^{(1)} = k_{y1}$ but because Nairn (2017) rotated x and y for loading in direction 2, $k_{x2}^{(2)} = k_{y2}$ and $k_{y2}^{(2)} = k_{x2}$.

G calculations must differentiate properties with respect to crack area. In finite fracture mechanics analysis of cracking events, the required derivative must be a *discrete* derivative or be the *change* in the bracketed term in Eq. (19) divided by the *change* in area, ΔA, due to formation of a complete crack in one layer. A discrete derivative corresponds to formation of a new crack between two existing cracks. Mistaken use of a continuous derivative corresponds to a non-physical process where a set of periodically-spaced cracks all close and then reopen as new periodic cracks at a higher density. Experimental results demonstrate that discrete differentiation models for layer cracking work better than continuous derivative models (Nairn et al, 1993).

Because G depends on Eq. (18), it only applies to cracking in one layer. It can be used to analyze cracking in both layers by considering cracking events alternating between layers using energy release rate equations specific for each layer. Energy released by a crack in core layer 1 finds a discrete derivative with $\Delta A = 4t_1 b$ to derive:

$$G_a = \frac{\sigma_0^{*2} t_1 Y_a^2(f\rho_a,\rho_b,\xi)}{E_{11}^0} \tag{31}$$

where f is explained below and

$$Y_a^2(\rho_a,\rho_b,\xi) = \frac{E_{11}^0}{V_1}\rho_a\left[\left(\frac{\xi}{\sqrt{E_{11}\left(\frac{\rho_a}{2},\rho_b\right)}}+\frac{1-\xi}{\sqrt{E_{22}\left(\frac{\rho_a}{2},\rho_b\right)}}\right)^2-\left(\frac{\xi}{\sqrt{E_{11}(\rho_a,\rho_b)}}+\frac{1-\xi}{\sqrt{E_{22}(\rho_a,\rho_b)}}\right)^2\right] \tag{32}$$

Energy released by crack formation in both surface layers (to maintain symmetry) with $\Delta A = 4t_2 a$ is:

$$G_b = \frac{\sigma_0^{*2} t_1 Y_b^2(\rho_a,f\rho_b,\xi)}{E_{11}^0} \tag{33}$$

where

$$Y_b^2(\rho_a,\rho_b,\xi) = \frac{E_{11}^0}{V_2}\rho_b\left[\left(\frac{\xi}{\sqrt{E_{11}\left(\rho_a,\frac{\rho_b}{2}\right)}}+\frac{1-\xi}{\sqrt{E_{22}\left(\rho_a,\frac{\rho_b}{2}\right)}}\right)^2-\left(\frac{\xi}{\sqrt{E_{11}(\rho_a,\rho_b)}}+\frac{1-\xi}{\sqrt{E_{22}(\rho_a,\rho_b)}}\right)^2\right] \tag{34}$$

Equations (31) and (33) were written for analogy with conventional fracture mechanics analysis of energy release rate, G_{FM}, and stress intensity factor, K_{FM}, for crack propagation:

$$G_{FM} = \frac{\sigma^2 a Y^2(a/W)}{E} \qquad \text{and} \qquad K_{FM} = \sqrt{G_{FM}E} = \sigma Y(a/W)\sqrt{a} \tag{35}$$

where σ is applied stress, a is crack length, E is material modulus, and $Y(a/W)$ is a dimensionless fracture mechanics calibration function that accounts for specimen geometry (W is specimen width) (Williams, 1984). The crack length a in G_{FM} is the source of scaling effects in fracture. Imagine two cracked specimens with identical geometries but one scaled down to smaller size. Stress analysis shows these two specimens have identical magnitudes of internal stresses, but experiments and fracture mechanics modeling agree that the larger specimen fails at lower stress. The appearance of t_1 in Eqs. (31) and (33) means that between two otherwise-identical CLT panels, the panel with thicker layers will crack first. The uncracked panel modulus (E_{11}^0) was included to convert $Y_a(\rho_a,\rho_b,\xi)$ and $Y_b(\rho_a,\rho_b,\xi)$ into dimensionless calibration functions analogous to $Y(a/W)$ in conventional fracture mechanics.

In Eq. (31) and Eq. (33), ρ_a and ρ_b are *average* crack spacings in the panel layers, but the energy analysis needs to use the crack spacing for the unit cell size that actually cracks. Because larger crack intervals release more energy than smaller ones, the next crack tends to form in unit cells that are larger than average. This tendency which is a consequence of current crack spacing distribution, can accurately be modeled by scaling the average density by the

Table 2 The mechanical and expansion properties used for timber in all calculations and derived from Douglas fir properties. The calculations were for flat-sawn timber with L, R, and T indicating longitudinal, radial, or tangential directions, respectively. CME units are strain per weight fraction water.

Property	Value	Property	Value	Property	Value	Property	Value
E_L	8.0 GPa	E_T	0.62 GPa	E_R	0.96 GPa	G_{LR}	0.8 GPa
G_{TR}	0.08 GPa	ν_{LT}	0.532	ν_{LR}	0.427	ν_{TR}	0.35
α_L	0.0	α_T	40×10^{-6} K^{-1}	β_L	0.0	β_T	0.26 wt^{-1}

above f factor and using $f > 1$ (Nairn et al, 1993; Nairn and Hu, 1994). Imagine N exactly periodic cracks spanning a length L. The i^{th} cracking event among the next N events ($i = 1$ to N) will form in one of the remaining uncracked intervals of length L/N while average crack density when it forms is $L/(N+i-1)$ or $f_i = (N+i-1)/N$. The average value of f for these events is:

$$\langle f\rangle = \frac{1}{N}\sum_{i=1}^{N}\frac{N+i-1}{N} = 1.5 - \frac{1}{2N} \tag{36}$$

By this simple analysis of sequential cracking, f is expected to range from 1 to 1.5 and asymptotically approach 1.5 for large N. Experimental results for f find typical values of $f = 1.2$ to 1.3 (Nairn et al, 1993). Recently, some authors failed to recognize the need to use f to account for distributions of crack spacings and erroneously suggested the discrete derivative approach is not accurate (Lim and Li, 2005). Experiments have confirmed, however, that both a discrete derivative *and* an accounting of distribution of crack spacings (*e.g.*, using the f factor) are essential for analysis of layer cracking (Nairn et al, 1993).

3 Cracking Prediction Results

This section uses finite fracture mechanics to predict CLT cracking under various loading situations. The analysis is general, but these calculations assumed a three-layer CLT panel made with identical core and surface layer properties. The timber was assumed to be flat-sawn such that *x*-*y*-*z* directions in layer 1 are approximately the tangential (T), longitudinal (L), and radial (R) directions in wood; table 2 lists the assumed properties. Finally, for identical layers, the residual stress terms simplify to:

$$\Delta_0 = \Delta_0' = \frac{(\alpha_T + \nu_{LT}\alpha_L)\Delta T + (\beta_T + \nu_{LT}\beta_L)\Delta c}{1+\nu_{LT}} \quad \text{and} \quad \Delta_1 = \Delta_2 = \frac{\big((\alpha_T - \alpha_L)\Delta T + (\beta_T - \beta_L)\Delta c\big)E_L}{1+\nu_{LT}} \tag{37}$$

3.1 Cracking Calibration Functions

Figure 2 plots $Y_a(\rho_a,\rho_b,\xi)$ and $Y_b(\rho_a,\rho_b,\xi)$ for various conditions as a function of dimensionless crack density $(1/\rho)$. Each group of three curves (indicated with arrows) corresponds to crack spacing in the other layer being $\rho = \infty$ (no cracks) or $\rho = 4$. For as-made CLT with non-glued edges, ρ is aspect ratio of the timber cross section (width/thickness). Setting $\rho = 4$ corresponds approximately to CLT made from $2'' \times 6''$ timber (with nominal dimensions 38×139 mm). The three curves in each group are for $\xi = 1$ (solid lines), 2/3 (dotted lines), and 0 (dashed lines). $\xi = 1$ and 0 correspond to pure mechanical load in the 1 or 2 directions. $\xi = 2/3$ corresponds to three-layer CLT with identical layers subjected only to residual stresses or $\xi = \sigma_1^*/\sigma_0^* = V_2 = 2/3$.

All calibration functions have the same shape as analogous functions for 2D layer cracking (Nairn, 1989, 1995). At low crack density, the functions are constant. This region corresponds to the conditions to initiate cracking. The horizontal plateaus at low crack density implies that once cracking starts, the next cracks form in rapid succession (because G remains critical). At higher crack density, all functions monotonically decrease, which predicts cracking rate slows at higher crack density. Both these predictions correspond to experimental observations (Nairn and Hu, 1994; Nairn, 2000). Varying ξ from 0 to 1 within each group maintains a rather high calibration function for forming cracks in either direction, including for cracks with their plane parallel to the loading direction. Both Y_a and Y_b increase as ρ in the other layer changes from ∞ to 4. In other words, cracks in either layer promote cracking in the other layer. Cracks in the other layer also change relative energy release rate as a function of ξ and reduce its influence. Finally,

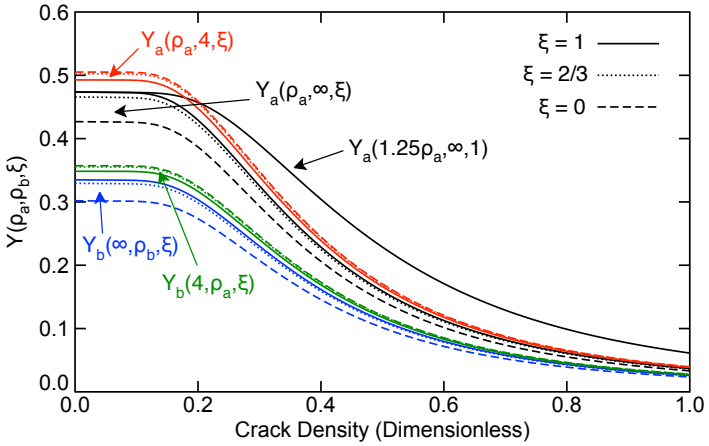

Fig. 2 Plots of $Y_a(\rho_a,\rho_b,\xi)$ as a function of $1/\rho_a$ and $Y_b(\rho_a,\rho_b,\xi)$ as a function of $1/\rho_b$. The two groups of Y_a plots are for $\rho_b \to \infty$ and $\rho_b = 4$ and for Y_b are for $\rho_a \to \infty$ and $\rho_a = 4$. Within each group, solid, dotted, and dashed lines are for $\xi = 1$, 2/3, and 0, respectively. The $Y_a(1.25\rho_a,\infty,1)$ curve shows the effect of $f = 1.25$ on one calibration function.

the $Y_a(1.25\rho_a,\infty,1)$ curve illustrates the effect of f factor used to account for non-periodic crack spacings. The plateau level is unaffected, but the monotonic decrease is slowed. As a result, real-world cracking initiates at loads that are independent of f but develops more cracks at high crack density.

3.2 Biaxial Cracking due to Residual Stresses Alone

Finite fracture mechanics analysis asserts that the next layer crack forms when total energy released by that crack equals the toughness of wood for a layer cracking event. For a panel experiencing only residual stresses ($\sigma_{10} = \sigma_{20} = 0$), cracks form in core or surface layer, respectively, when

$$-V_2\Delta_2 - V_1\Delta_1 = \frac{1}{Y_a(f\rho_a,\rho_b,\xi_{res})}\sqrt{\frac{G_{Lc}^{(1)}E_{11}^0}{t_1}} \quad \text{or} \quad -V_2\Delta_2 - V_1\Delta_1 = \frac{1}{Y_b(\rho_a,f\rho_b,\xi_{res})}\sqrt{\frac{G_{Lc}^{(2)}E_{11}^0}{t_1}} \tag{38}$$

where $G_{Lc}^{(k)}$ is the layer cracking event toughness for layer k and $\xi_{res} = V_2\Delta_2/(V_2\Delta_2 + V_1\Delta_1)$. $G_{Lc}^{(k)}$ is a new material property for wood. Ideally it would be measured by experiments described below. It is likely close to the toughness to initiate cracks running parallel to wood grain (known as "RL" or "TL" toughness (Schniewind and Centeno, 1973)). Typical values for wood range from 50 to 400 J/m^2 depending on species (Shir Mohammadi and Nairn, 2014; Wilson et al, 2013). For flat-sawn, Douglas fir used here, G_{Lc} might be close to the toughness to initiate TL fracture that ranges from 120 to 220 J/m^2 (Matsumoto and Nairn, 2012; Wilson et al, 2013).

A progressive failure analysis can predict residual stress cracking. CLT with non-glued edges starts as a pre-cracked panel with initial crack spacings ρ_a and ρ_b equal to timber cross-section aspect ratios. If such a panel has $G_{Lc}^{(1)} = G_{Lc}^{(2)}$ and equilibrium residual stresses, cracking will start in the core layer because Fig. 2 shows that Y_a is always greater than Y_b. As cracking proceeds, Y_a decreases while Y_b slightly increases. When Y_a reaches Y_b, cracking will start in the surface layers as well. Once both layers are cracking, subsequent cracking will follow a path that maintains $Y_a = Y_b$. Imagine 3D surface plots of Y_a and Y_b as a function of ρ_a and ρ_b. Residual stress cracking will start along the Y_a surface until it intersects the Y_b surface. Thereafter, it will follow the intersection of the two surfaces. The minus signs mean cracking only occurs when a combination of temperature and moisture change gives $-V_2\Delta_2 - V_1\Delta_1 > 0$ (*i.e.*, residual shrinkage). This analysis is easily generalized to $G_{Lc}^{(1)} \neq G_{Lc}^{(2)}$ and to non-equilibrium moisture content and which layer cracks first may change. The effects of moisture gradients when drying is briefly discussed below.

Figure 3 gives predictions of residual stress cracking for panels made from identical layers ($V_1 = 1/3$, $\Delta_1 = \Delta_2$, and $\xi = 2/3$) using properties in Table 2, $G_{Lc}^{(k)} = 150$ J/m^2, and $f = 1.25$. These calculations assumed residual stresses were caused by moisture change alone ($\Delta T = 0$). Calculated results for Δ_1 were converted to precent moisture decrease

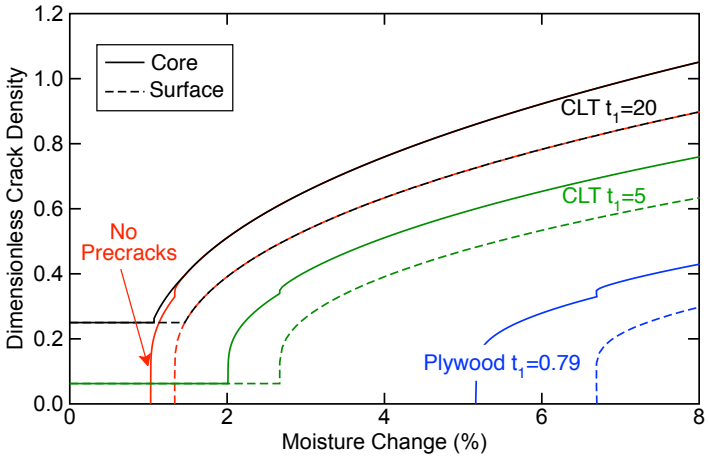

Fig. 3 The predicted dimensionless crack density in core and surface layers as a function of moisture change (positive means decrease in moisture content) for three different cross-laminated products. The "CLT t_1=20" curves are for typical CLT made from 40×160 mm timber. The "CLT t_1=5" curves is made from thinner timber layers. The "Plywood" curves use $2 \times 0.79 = 1.58$ mm veneer layers. The two curves labeled "No Precracks" are for a CLT panel with no initial cracks (*i.e.*, very wide timber or glued edges).

using $\Delta c(\%) = 100\Delta_1(1+\nu_{Lt})/(E_L(\beta_T - \beta_L))$. The CLT was assumed to be made from 160 mm wide timber. The "CLT $t_1 = 20$" curves thus corresponds approximately to CLT made from $2'' \times 6''$ timber. At first, the dimensionless crack density remains constant at the precrack density of $20/80 = 0.25$ mm^{-1}. At about 1% moisture change the core layer starts to crack. The surface layers start cracking at about 1.5% moisture change. As moisture change increases the core and surface layers continue to crack at similar rates.

The other curves in Fig. 3 examine residual stress cracking in modified CLT panels. The "No Precracks" curves is for a CLT panel made with impossibly-wide timber or by gluing edges within layers. This change has very little effect on eventual panel cracking. Soon after crack initiation, the crack density in a panel with no cracks equals the crack density of a panel with non-glued edges. The kink in the core layer curve with no precracks is caused by the sudden decrease in ρ_b once surface layer cracking starts; this decreases causes step change in Y_a for core layer cracking (see Fig. 2).

Because G_a and G_b scale with panel thickness, two examples considered CLT with thinner layers. As expected, the moisture change required to initiate cracking scales as $1/\sqrt{t_1}$. Thus moisture change needed to initiate cracking is doubled with 5 mm layers and is increased five fold in plywood ($t_1 = 0.79$ mm). By varying surface and core layer properties, additional plywood cracking predictions would provide a tool for modeling veneer checking of plywood (Batey, 1955). The dimensioned crack density (*i.e.* number of cracks per unit length) is equal to dimensionless crack density divided by $2t_1$. Thus, although thinner layers can suppress cracking, once cracking starts, they can develop more cracks. Because Eq. (21) shows property degradation depends on ρ, however, plots of dimensionless crack spacing are the preferred metric for monitoring damage caused by cracks. This approach might need to change for properties affected by absolute number of cracks (*e.g.*, appearance or acceleration of moisture update).

3.3 Uniaxial Tensile Loading at Constant Residual Stresses

For uniaxial tensile loading in direction 1, finite fracture mechanics predicts the load to induce the next crack in the core or surface layers, respectively, is:

$$\sigma_{10} = \frac{1}{Y_a(f\rho_a,\rho_b,\xi_1)}\sqrt{\frac{G_{Lc}^{(1)}E_{11}^0}{t_1}} + V_2\Delta_2 + V_1\Delta_1 \quad \text{or} \quad \sigma_{10} = \frac{1}{Y_b(\rho_a,f\rho_b,\xi_1)}\sqrt{\frac{G_{Lc}^{(2)}E_{11}^0}{t_1}} + V_2\Delta_2 + V_1\Delta_1 \tag{39}$$

where $\xi_1 = (\sigma_{10} - V_2\Delta_2)/(\sigma_{10} - V_2\Delta_2 - V_1\Delta_1)$. These equations could be used to predict cracking in both layers as load increases. An interesting special case, which is proposed here as a method to measure $G_{Lc}^{(1)}$, is to use a sufficiently narrow width W in direction 2 such that $Y_b(\rho_a, fW/(2t_1), \xi_1)$ is always less than $Y_a(f\rho_a, W/(2t_1), \xi_1)$. For such a

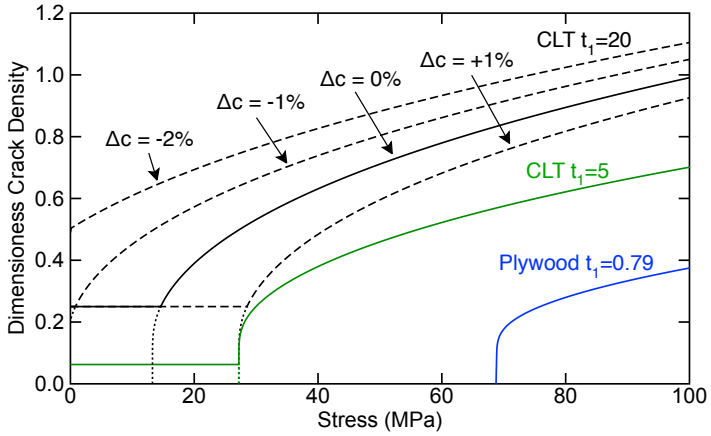

Fig. 4 The predicted dimensionless crack density in the core layer as a function applied stress for three different cross-laminated products. The four "CLT t_1=20" curves are for typical CLT made from 40×160 mm timber. The "CLT t_1=5" curve is made from thinner timber layers. The "Plywood" curve use $2 \times 0.79 = 1.58$ mm veneer layers. The dashed curves show the change in the "CLT t_1=20" results for panels have various amounts of moisture content change (Δc) before testing.

specimen, loading will crack only the core layer. Uniaxial tension experiments can be fast enough that Δ_1 and Δ_2 remain constant, but their values depend on how the panel was made and on its environmental history.

Figure 4 gives predictions of core layer cracking by uniaxial loading of narrow panels ($W = 100$ mm) made from identical layers ($V_1 = 1/3$, $\Delta_1 = \Delta_2$, timber width = 160 mm) using properties in Table 2, $G_{Lc}^{(1)} = 150$ J/m^2, and $f = 1.25$. To find ξ_1, calculations started with an initial guess (between 2/3 and 1) to find a provisional σ_{10}. This value was then recursively used to refine ξ_1 until calculated σ_{10} became constant (very few recursions were needed; none when $\Delta_1 = 0$). Because mechanical and residual stresses both cause cracking, these curves are similar to the residual stress cracking curves in Fig. 3. The solid curves are for panels with $\Delta_1 = 0$, which corresponds to panels made at room temperature with timber at equilibrium moisture content and then immediately tested. The horizontal segments for CLT panels with $t_1 = 20$ or 5 mm correspond to initial crack density determined by timber width. The dotted extensions of these curves show expected results for panels with glued edges. Such panels would reach the same amount of layer cracking soon after cracking initiates. Because of thickness scaling, the stress to initiate layer cracking doubles when $t_1 = 5$ mm and increases five fold for plywood. The stress to initiate cracking in plywood exceeds its tensile strength (Forest Products Laboratory, 2010). In other words, one would never see layer cracking in plywood before the entire panel failed by axial wood failure.

The three dashed curves in Fig. 4 show effects of adding residual stresses for panels experiencing $\pm 1\%$ or -2% moisture change between the time the panels are made and tensile experiments are run. Residual stresses shift the curves left for moisture decrease or right for increase. As seen in Fig. 3, core layer cracking due solely to residual stresses starts at about 1% moisture change. Thus panels with more than 1% decrease in moisture content will develop cracks *before* testing causing the crack density curves at zero stress to start above the precrack density. A panel with moisture increase ($\Delta c = +1\%$) shifts initiation stress the same amount as reducing layer thickness by a factor of four. Thinner layers, however, are more effective at reducing subsequent cracking rates than moisture increases.

Uniaxial tensile testing could be used to measure $G_{Lc}^{(1)}$. A recommended experimental program is to make a series of CLT panels that vary thicknesses of core layer, surface layer, or both layers. If panels are made with a room-temperature cure adhesive and tested at room temperature, the thermal shrinkage term should be $\Delta T = 0$. Accounting for only moisture shrinkage and for layers with the same properties, the failure load prediction can be cast as:

$$\sigma_{10} = D_R \sqrt{G_{Lc}^{(1)}} + \frac{(\beta_T - \beta_L) E_L}{1 + \nu_{Lt}} \Delta c \quad \text{where} \quad D_R = \frac{1}{Y_a\left(\frac{f}{2D_a t_1}, \frac{W}{2t_1}, \xi_1\right)} \sqrt{\frac{E_{11}^0}{t_1}} \tag{40}$$

is a reduced crack density calculated from the counted cracks per unit length, D_a, and the calibration function. These experiments would monitor D_a in the core layer as a function of applied stress σ_{10}. A plot of σ_{10} *vs.* D_R should be a straight line with slope as an experimental result for $G_{Lc}^{(1)}$ and intercept as an experimental result for *effective* moisture

change that has occurred since panel fabrication. Because both slope and intercept are independent of t_1 and V_1, a collection of panels with variable t_1 and V_1 should all fall on the same line, which would provide many data points for determining $G_{Lc}^{(1)}$. Such experiments could also monitor toughness and moisture changes over time. Imagine a series of specimens exposed to different environmental histories followed by core cracking experiments. Slope changes would reveal changes in $G_{Lc}^{(1)}$ while intercept changes would reveal changes in effective Δc.

A similar "master plot" method successfully correlates many experiments on cross-ply laminates with variable ply thickness (Nairn et al, 1993). One difference needs comment. The Y_a calibration function needed to find D_R depends on σ_{10} and Δ_1 through the ξ_1 term. The comparable terms in 2D microcracking do not have such dependencies (Nairn et al, 1993). Fortunately, Y_a, is only weakly dependent on ξ_1 and it only varies within the narrow range of V_2 to 1. It should be acceptable to set it to any value in this range or just use $\xi_1 = 1$ if mechanical loads dominate the test.

4 Discussion

CLT layer cracking is neither desirable nor ignorable. Formation of new cracks over time degrades the panel's mechanical properties. In-plane tensile moduli degrade little, but in-plane shear modulus will tend to zero at high crack density (Bogensperger et al, 2010; Nairn, 2017). Layer cracks have other consequences as well. Cracks in surface layers degrade the appearance of exposed panels. Intersections of layer cracks with bond lines between layers can nucleate adhesive bond failure or delaminations (Nairn and Hu, 1992). Nearly all wood product failures are associated with unwanted moisture or biodegradation (Zabel and Morrell, 2012). Layer cracks provide pathways that accelerate moisture uptake into panels thereby allowing moisture penetration into panel depths that otherwise would not occur.

The design of CLT structures should consider all effects of layers cracks forming over time and their role in CLT durability. Finite fracture mechanics concepts combined with energy release rate equations derived here (Eqs. (19), (31), and (33)) provide tools for developing improved CLT panels or designing durable CLT structures. This section briefly considers several topics and suggests areas for future analysis or experiments.

4.1 Redesigning CLT to Suppress Cracks

The simplest change to suppress cracking is to use thinner layers. Each factor of four reduction in thickness doubles the stress required to initiate cracks and reduces the dimensionless crack spacing that can develop in layers. Given $G_{Lc}^{(k)}$, one could calculate the thickness required such that a panel would fail by other mechanisms before layers start to crack. For example, Fig. 4 predicts that plywood veneers are thin enough to suppress cracking. Experiments on glass/epoxy composites confirm that thin-layer, crack suppression methods work (Parvizi et al, 1978).

A plan to ameliorate effects of non-glued edges acting as precracks or to delay formation of new cracks by edge-gluing the timber is predicted to be ineffective. All calculations with typical dimensions and wood properties predict that soon after cracking starts, a panel with glued edges develops the same level of cracking as a panel with non-glued edges. An analogy can be drawn to concrete slabs where a plan to edge-glue timber corresponds to pouring a slab with no expansion joints. Such a slab would crack just as much as a slab with expansion joints. A plan to combine thinner layers with edge gluing, however, is promising. If layers are thin enough to suppress cracks, edge gluing could eliminate deleterious effects caused by non-glued edges acting as the only remaining cracks.

4.2 Using Structural Loads to Suppress Cracks

The σ_0^{*2} term in Eq. (19) suggests that cracks form under tension and compression, but that interpretation is wrong. The general equation applies to both tension and compression, but only if the $E_{11}(\rho_a,\rho_b)$ and $E_{22}(\rho_a,\rho_b)$ analyses are non-linear analyses that account for differences between opened and closed cracks. The analyses in Hashin (1987) and Nairn (2017) both assume stress-free crack surfaces and therefore only apply when cracked layers are in tension. A non-conservative, non-linear analysis would be to assume that cracks in compression act as if they disappear. A

simple, non-linear analysis for in-plane moduli could be:

$$\frac{1}{E_{11}(\rho_a,\rho_b)} = \begin{cases} \frac{1}{E_{11}^0} + \frac{V_1\chi_1(\rho_a,\rho_b)}{\rho_a\rho_b} & \text{for } \overline{\sigma_{xx}^{(1)}} > 0 \text{ and } \overline{\sigma_{yy}^{(2)}} > 0 \\ \frac{1}{E_{11}^0} + \lim\limits_{\rho_b\to\infty} \frac{V_1\chi_1(\rho_a,\rho_b)}{\rho_a\rho_b} & \text{for } \overline{\sigma_{xx}^{(1)}} > 0 \text{ and } \overline{\sigma_{yy}^{(2)}} < 0 \\ \frac{1}{E_{11}^0} + \lim\limits_{\rho_a\to\infty} \frac{V_1\chi_1(\rho_a,\rho_b)}{\rho_a\rho_b} & \text{for } \overline{\sigma_{xx}^{(1)}} < 0 \text{ and } \overline{\sigma_{yy}^{(2)}} > 0 \\ \frac{1}{E_{11}^0} & \text{for } \overline{\sigma_{xx}^{(1)}} < 0 \text{ and } \overline{\sigma_{yy}^{(2)}} < 0 \end{cases} \tag{41}$$

with an analogous form for $E_{22}(\rho_a,\rho_b)$. This approach is non-conservative because cracks may not completely close (*e.g.*, due to surface damage or gaps) or structural shear stresses may cause slippage (*e.g.*, a layer with closed cracks may respond to shear differently than an uncracked layer). Substituting nonlinear $E_{11}(\rho_a,\rho_b)$ and $E_{22}(\rho_a,\rho_b)$ into Eq. (19) predicts that cracks will not occur when $\overline{\sigma_{xx}^{(1)}} < 0$ and $\overline{\sigma_{yy}^{(2)}} < 0$ because that causes $G = 0$

One method to prevent cracks caused by residual stresses is to avoid exposure to net shrinkage due to temperature and moisture changes. Residual stresses are controlled by ΔT and Δc that are *changes* in temperature or moisture relative to a reference, stress-free state. For CLT panels, the reference state is approximately the temperature and moisture content of the timber at the time layers are bonded. Because adhesive chemistry determines bonding temperature, ΔT is difficult to control. But, all things being equal, a low-temperature cure adhesive would result in lower thermal residual stresses than a high-temperature cure adhesive. Controlling Δc is easier. One method is to pre-dry all timber to a moisture content *below* the lowest moisture content the panel might see in service. This method's motivation is to maintain $\Delta c > 0$ throughout the panel's life.

A centuries-old use of residual stresses to improve durability of steel blades is to quench or hammer the surfaces to induce compressive residual stresses (Cheng and Finnie, 2007). Could a similar approach improve CLT durability? For example, instead of drying all layers to low moisture content, what if only surface layers were dried? Simple calculations show this method would induce compression in surface layers that could inhibit cracking, but unfortunately it would cause tensile stress in the core layer (see *Online Resource*). The extra cracks that could form in a core layer would still degrade mechanical properties although shear modulus would not degrade as much as when all layers crack (Nairn, 2017). Compared to drying all layers to low moisture content, drying only surface layers provides very little benefit in surface compression stress and causes detrimental tensile stress in core layers. If some layers are dried to low moisture content, all layers might as well be dried.

Cracks might be suppressed by keeping panels constantly compressed. Obviously, compression in direction 1 compresses layer 1 in that same direction, but composite plate analysis shows that direction 1 compression also induces transverse compression in layer 2. To find compression stress required to close all cracks, it suffices to analyze a CLT panel with no cracks. Assuming a linear elastic analysis, transverse layer stresses can be written as

$$\overline{\sigma_{xx}^{(1)}} = k_{x1}^{(1)}\sigma_{10} + k_{x2}^{(1)}\sigma_{20} + k_{th,1}\Delta T + k_{c,1}\Delta c \quad \text{and} \quad \overline{\sigma_{yy}^{(2)}} = k_{y1}^{(2)}\sigma_{10} + k_{y2}^{(2)}\sigma_{20} + k_{th,2}\Delta T + k_{c,2}\Delta c \tag{42}$$

where influence coefficients for an uncracked laminate are:

$$\begin{pmatrix} k_{x1}^{(k)} & k_{x2}^{(k)} \\ k_{y1}^{(k)} & k_{y2}^{(k)} \end{pmatrix} = \begin{pmatrix} Q_{xx}^{(k)} & Q_{xy}^{(k)} \\ Q_{xy}^{(k)} & Q_{yy}^{(k)} \end{pmatrix} \begin{pmatrix} 1/E_{11}^0 & -\nu_{12}^0/E_{11}^0 \\ -\nu_{12}^0/E_{11}^0 & 1/E_{22}^0 \end{pmatrix}, \tag{43}$$

$$k_{th,1} = \left(\alpha_{11}^0 - \alpha_{xx}^{(1)}\right)Q_{xx}^{(1)} + \left(\alpha_{22}^0 - \alpha_{yy}^{(1)}\right)Q_{xy}^{(1)}, \text{ and } k_{th,2} = \left(\alpha_{11}^0 - \alpha_{xx}^{(2)}\right)Q_{xy}^{(2)} + \left(\alpha_{22}^0 - \alpha_{yy}^{(2)}\right)Q_{yy}^{(2)} \tag{44}$$

and $k_{c,i}$ is found by analogy to $k_{th,i}$ using CMEs. The uncracked thermal expansion properties are given by substituting E_{11}^0, E_{22}^0, and ν_{12}^0 into Eqs. (9) and (13). The mechanical stresses that suppress cracks in layers 1 and 2 are:

$$\sigma_S^{(1)} = -\frac{k_{th,1}\Delta T + k_{c,1}\Delta c}{k_{x1}^{(1)}\xi_m + k_{x2}^{(1)}(1-\xi_m)} \quad \text{and} \quad \sigma_S^{(2)} = -\frac{k_{th,2}\Delta T + k_{c,2}\Delta c}{k_{y1}^{(2)}\xi_m + k_{y2}^{(2)}(1-\xi_m)} \tag{45}$$

where $\sigma_S^{(i)} = \sigma_{10} + \sigma_{20}$ and $\xi_m = \sigma_{10}/\sigma_S^{(i)}$. For one example, consider a panel with identical layers of flat-sawn timber experiencing $\Delta c = -1\%$ moisture change alone ($\Delta T = 0$). The stresses required to suppress cracks in core and surface layers are $\sigma_S^{(1)} = -13.1$ MPa and $\sigma_S^{(2)} = -27.6$ MPa. The stresses required to overcome just 1% moisture content change are a significant fraction of the mean compression strength of CLT (38.7 ± 1.6 MPa (Oh et al, 2015)). Expecting compression in structures, such as walls, to prevent cracks is probably unrealistic.

4.3 Durability Analysis Methods

While Eq. (19) predicts static conditions to cause a crack, it says nothing about fatigue cracking caused by oscillations at subcritical loads or residual stresses. The usual fracture mechanics approach to fatigue analysis of crack propagation is to use a Paris et al (1961) law:

$$\frac{da}{dN} = A\Delta K_{FM}^m \tag{46}$$

where da/dN is crack growth rate per cycle and ΔK_{FM} is variation of crack-tip stress intensity factor in each cycle. A and m are two material properties that can be used to predict fatigue life. They are measured from intercept and slope of log-log plots for da/dN as a function of ΔK_{FM}. Finite fracture mechanics of CLT cracking can use Paris-law methods by replacing crack length with crack density and stress intensity factor with cracking energy release rates:

$$\frac{dD_a}{dN} = A_1\Delta G_a^{m_1} \qquad \text{and} \qquad \frac{dD_b}{dN} = A_2\Delta G_b^{m_2} \tag{47}$$

where dD_a/dN and dD_b/dN are rates of crack density increase in core and surface layers and A_k and m_k are two new wood material properties characterizing durability of layer k with respect to cracking. Quantitative predictions of long-term cracking in CLT should be based on measured A_k and m_k and integrations of Eq. (47) using Eqs. (31) and (33) up to design limits for D_a and D_b. In principle, A_k and m_k can be measured by mechanical, thermal, or moisture cycling. The results, however, may differ if $G_{Lc}^{(k)}$ varies with temperature and moisture. A few such experiments were done on cross-ply, carbon/epoxy laminates and they fit a modified Paris-law well (Liu and Nairn, 1990; Nairn, 1992). These experiments measured $m_k = 5.5$ during mechanical cycling and $m_k = 6.7$ during thermal cycling. Because G_a and G_b scale with thickness, a Paris-law analysis suggests CLT durability scales with $t_1^{m_k}$. If m_k for wood is as high as m_k for carbon/epoxy laminates, thinner layers could enhance CLT durability more dramatically than the $t_1^{1/2}$ scaling implied by static cracking analysis.

4.4 Delamination

Layer cracks typically arrest when they reach an interface with an adjacent layer. But intersections between layer cracks and interfaces cause stress concentrations that can promote interfacial failure or delamination. In CLT, this delamination would be wood/adhesive bond failure between timber faces. Layer-crack-induced delaminations are observed in aerospace composites (Crossman and Wang, 1982; Crossman et al, 1980), particularly on panel edges (O'Brien, 1985, 1984). When delaminations start, they dominate over layer cracking and cause more significant property degradation. In fact, delamination onset may be the prime factor in limiting composite durability (Gilchrist et al, 1996). The design of durable CLT structures should be informed by an understanding of conditions that cause layer cracks to turn into delaminations.

Delamination prediction is a conventional crack-propagation problem that can be modeled by finding energy release rate for delamination growth from tip of a layer crack, G_D, as a function of layer crack spacing, ρ. Although no 3D model for this energy release rate is available, a 2D result for G_D (Nairn and Hu, 1992) provides some information. Like G_a and G_b, G_D scales with layer thickness. Thus, the thick layers in CLT promote *both* layer cracking and delaminations. As crack density increases, G_D decreases, but it decreases slower than G_a and G_b. As a consequence, the predicted failure process is to start with layer cracks, but once G_a and G_b decrease to below G_D, layer cracks will turn into adhesive bond failures causing serious degradation to panel properties. The critical crack density for delamination onset depends on G_D and on relative toughness for wood cracking $G_{Lc}^{(k)}$ compared to adhesive bond-line toughness, G_{Bc}. 2D calculations predict that if $G_{Lc}^{(k)} = G_{Bc}$, delamination starts when dimensionless crack spacing is $1/\rho = 0.55$ (see *Online Resource* and Nairn and Hu (1992)). This critical crack spacing increases or decreases with G_{Bc}. Thus an important role for CLT adhesive is to inhibit delamination onset by maximizing G_{Bc}. Future work should derive 3D results for G_D and measure both $G_{Lc}^{(k)}$ and G_{Bc}.

4.5 Other Issues

The analysis tools developed here can provide information about more issues and suggest new areas for research. A few are briefly described.

This paper considered in-plane loading that is most appropriate for CLT walls. In contrast, CLT floors are under bending loads. 2D analysis of layer cracking in bending is available (McCartney and Pierce, 1997; McCartney and Byrne, 2001; Kim and Nairn, 2000a,b); it should be extended to 3D cracking of CLT in bending. The probable findings would be that cracking is worse on the tension side of the panel and suppressed on the compression side. Delamination onset in floor panels would likely be more deleterious to performance than delaminations in wall panels.

In-plane normal stress analysis is ignoring shear stresses. Because thermal and moisture expansion only occur in normal strains (for orthotropic materials), energy released due to shear stress is decoupled from residual stress. Shear effects can be included with a new term in G_{mech}. Calculations reveal an extra energy released by shear loading of

$$G_{shear} = \frac{V\tau_{12}^2}{2}\frac{d}{dA}\left(\frac{1}{G_{12}(a,b)}\right) \tag{48}$$

where τ_{12} is applied in-plane shear stress and $G_{12}(a,b)$ is the panel's effective in-plane shear modulus (Nairn, 1997). Approximate theories for $G_{12}(a,b)$ (Bogensperger et al, 2010; Nairn, 2017) can be used to calculate shear energy contribution to energy release rate

The residual stresses were assumed to be caused by constant ΔT and Δc in all layers, which corresponds to panels at thermal and moisture equilibrium. This approach is appropriate for slow changes such as seasonal variations in temperature and moisture content. Analysis of sudden events (*e.g.*, relatively rapid changes in moisture content) might need additional modeling. The same finite fracture mechanics concepts can be used but would need numerical methods to account for gradients in temperature and moisture within a panel. For example, panel drying would dry surface layers before core layers. The developed gradients might promote cracking in surface layers before core layers, which is opposite of predictions above for equilibrium content in all layers.

ΔT and Δc are calculated from a reference state and some calculations here assumed that state to be the temperature and moisture content at the time the faces are bonded. This approach assumes linear, hygro-thermal elasticity; nonlinear effects, such as viscoelastic relaxations, might change the reference state. For example, imagine a CLT structure exposed to significant moisture during construction (such as rain events). The added moisture will swell the panels resulting in compression that suppresses cracks during construction. But, if wood softening at higher moisture content relaxes residual stresses, the panel's reference moisture content might shift to a higher value. As a result, moisture shrinkage *after* construction would cause more cracks than in panels protected from rain during construction. Shifts in reference state due to weather exposure could be observed experimentally as shifts in intercepts from experiments on uniaxial core-layer cracking (see above).

The wood cracking toughness, $G_{Lc}^{(k)}$, is an important material property that should be measured. It is likely similar to fracture toughness of wood for cracks parallel to the wood grain and that toughness depends on orientation of the crack normal with respect to the growth rings. The energy driving layer cracks promotes cracks with surface normal in the plane of the panel. Thus the crack normal in flat-sawn timber would be in the tangential direction (a TL crack) while for radial-sawn timber would in the radial direction (a RL crack). Timber with curved growth rings would get cracks between RL and TL cracks. Fracture experiments on wood show that crack initiation parallel to wood grain is insensitive to growth ring orientation (Johnson, 1973; Schniewind and Centeno, 1973; Reiterer et al, 2000; Fruhmann et al, 2002), but if experiments are continued into crack propagation, TL toughness is significantly higher than RL toughness (Matsumoto and Nairn, 2012; Wilson et al, 2013). The increase in toughness is due to fiber bridging effects (Mirzaei et al, 2016). Experiments to measure $G_{Lc}^{(k)}$ as a function of end-grain patterns could determine if layer cracks are influenced by crack normal direction. If fiber bridging contributes to $G_{Lc}^{(k)}$, CLT properties would be improved by using only flat-saw timber and avoiding timber from near the pith.

An interesting option might be to include angled layers (*e.g.*, at $\pm 45^\circ$) in CLT panels. Angled plies may not inhibit cracks (cracking of angled plies in aerospace composites is observed (Salpekar and O'Brien, 1991; Hu et al, 1993)), but they may ameliorate property degradation. For example, effective layer analysis (Nairn, 2017) attributing zero transverse stiffness to cracked layers predicts that a CLT panel with angled plies would retain useful shear stiffness while a panel with only 0° and 90° layers would tend to zero shear stiffness. After delamination onset, angle-ply layers may provide little benefit and may even exacerbate edge delaminations (Crossman and Wang, 1982; Crossman et al, 1980).

5 Conclusions

An understanding of cracking and delamination in CLT panels is a prerequisite to the design of durable structures. The energy release rate analysis derived here can be a basis for that understanding. Additional modeling is needed to predict onset of delaminations. Making quantitative predictions of cracking rates or structural lifetimes requires input of new material properties. The most important properties are layer cracking toughness, $G_{Lc}^{(k)}$, adhesive bond toughness, G_{Bc}, and Paris-law fatigue properties, A_k and m_k. Experimental methods for measuring these properties were described.

The sample calculations done here suggest current CLT panels are prone to cracks. As little as 1% moisture content decrease after fabrication is enough to start cracking and 2-3% decrease might result in serious damage and delaminations. Finite fracture mechanics analysis can be a design tool for developing and assessing strategies for improving CLT performance. Some readers might complain that the rather simple recommendations outlined here — using thinner layers, sufficiently drying the timber, gluing edges (but only if using thin, dry layers), and optimizing end-grain patterns — would increase the cost of CLT panels. But if cost analysis includes the cost of replacing a building with cracked CLT panels, redesigning CLT panels before constructing buildings could be the lowest-cost approach.

Acknowledgements This work was made possible by the endowment for the Richardson Chair in Wood Science and Forest Products.

References

Batey TEJ (1955) Minimizing face checking of plywood. Forest Products Journal 5(10):277–284

Bogensperger T, Moosbrugger T, Silly G (2010) Verification of clt-plates under loads in plane. In: World Conference on Timber Engineering, June 20-24, Riva del Garda, Italy

Cheng W, Finnie I (2007) Residual Stress Measurement and the Slitting Method. Springer US, Boston, MA

Christenson RM (1979) Mechanics of Composite Materials. John Wiley & Sons, New York

Crossman FW, Wang ASD (1982) The dependence of transverse cracking and delamination on ply thickness in graphite/epoxy laminates. ASTM STP 775:118–139

Crossman FW, Warren WJ, Wang ASD, G E Law J (1980) Initiation and growth of transverse cracks and edge delamination in composite laminates: Part 2. experimental correlation. J Comp Mat Supplement 14:89–108

Forest Products Laboratory (2010) Wood handbook: wood as an engineering material. General technical report FPL-GTR-190. Madison, WI: U.S. Dept. of Agriculture, Forest Service, Forest Products Laboratory

Fruhmann K, Reiterer A, Tschegg EK, Stanzl-Tschegg SS (2002) Fracture characteristics of wood under mode i, mode ii and mode iii loading. Philosophical Magazine A: Physics of Condensed Matter, Structure, Defects and Mechanical Properties 82(17-18):3289–3298

Gent AN (1990) Cavitation in rubber: A cautionary tale. Rubber Chemistry and Technology 63(3):49–53

Gent AN, Lindley PB (1959) Internal rupture on bonded rubber cylinders in tension. Proc Roy Soc Lond A 249:195–205

Gent AN, Wang C (1991) Fracture mechanics and cavitation in rubber-like solids. J Mat Sci 26(12):3392–3395

Gilchrist MD, Kinloch AJ, Mathews F, Osiyemi SO (1996) Mechanical performance of carbon- fibre- and glass-fibre-reinforced epoxy I-beams: I. Mechanical. Comp Sci & Tech 56:37–53

Groisman A, Kaplan E (1994) An experimental study of cracking induced by desiccation. Europhysics Letters 25(6):415

Hashin Z (1987) Analysis of orthogonally cracked laminates under tension. J Appl Mech 54:872–879

Hashin Z (1996) Finite thermoelastic fracture criterion with application to laminate cracking analysis. Journal of the Mechanics and Physics of Solids 44:1129–1145

Hu S, Bark JS, Nairn JA (1993) On the phenomenon of curved microcracks in $[(S)/90_n]_s$ laminates: Their shapes, initiation angles, and locations. Comp Sci & Tech 47:321–329

Johnson JA (1973) Crack initiation in wood plates. Wood Science 6(2):151–158

Kim SR, Nairn JA (2000a) Fracture mechanics analysis of coating/substrate systems subjected to tension or bending loads I: Theory. Engr Fract Mech 65:573–593

Kim SR, Nairn JA (2000b) Fracture mechanics analysis of coating/substrate systems subjected to tension or bending loads II: Experiments in bending. Engr Fract Mech 65:595–607

Leterrier Y, Andersons J, Pitton Y, Månson JAE (1997a) Adhesion of silicon oxide layers on poly(ehtylene terepthalate). II Effect of coating thickness on adhesive and cohesive strengths. J Polym Sci, Part B: Polymer Physics 35:1463–1472

Leterrier Y, Boogh L, Andersons J, Månson JAE (1997b) Adhesion of silicon oxide layers on poly(ehtylene terepthalate). I: Effect of substrate properties on coating's fragmentation process. J Polym Sci, Part B: Polymer Physics 35:1449–1461

Leterrier Y, Fischer C, Médico L, Demarco F, Månson JAE, Bouten P, DeGoede J, Nairn JA (2003) Mechanical properties of transparent functional thin films for flexible displays. In: Proc. 46th Ann. Tech. Conf. Soc. Vacuum Coaters

Leterrier Y, Waller J, Manson JA, Nairn JA (2009) Models for saturation damage state in multilayer coatings. Mechanics of Materials 42:326–334

Levin VM (1967) On the coefficients of thermal expansion in heterogeneous materials. Mechanics of Solids 2:58–61

Lim SH, Li S (2005) Energy release rates for transverse cracking and delaminations induced by transverse cracks in laminated composites. Composites Part A 36:1467–1476

Liu S, Nairn JA (1990) Fracture mechanics analysis of composite microcracking: Experimental results in fatigue. In: Proc. of the Amer. Soc. of Comp., 5^{th} Tech. Conf., June 11-14, East Lansing, MI, USA, pp 287–295

Matsumoto N, Nairn JA (2012) Fracture toughness of wood and wood composites during crack propagation. Wood and Fiber Science 44(2):121–133

McCartney LN (1993) The prediction of cracking in biaxially loaded cross-ply laminates having brittle matrices. Composites 24:84–92

McCartney LN (2008) Energy methods for fatigue damage modelling of laminates. Composites Science and Technology 68:2601–2615

McCartney LN, Byrne MJW (2001) Energy balance method for predicting cracking in cross-ply laminates during bend deformation. In: Proc. 10th Int. Conf. on Fracture (ICF-10), Advances in Fracture Research, 2–6 December, Honolulu, HI, USA

McCartney LN, Pierce C (1997) Stress transfer mechanics for multiple ply laminates for axial loading and bending. In: Proc. ICCM-11, Gold Coast, Australia

Mirzaei B, Sinha A, Nairn JA (2016) Measuring and modeling fiber bridging: Application to wood and wood composites exposed to moisture cycling. Comp Sci & Tech 128:65–74

Nairn JA (1989) The strain energy release rate of composite microcracking: A variational approach. J Comp Mat 23:1106–1129

Nairn JA (1992) Microcracking, microcrack-induced delamination, and longitudinal splitting of advanced composite structures. Tech. rep., NASA Contractor Report 4472

Nairn JA (1995) Some new variational mechanics results on composite microcracking. In: Proc. 10^{th} Int'l Conf. on Comp. Mat., Vancover, BC, Canada, 1995, vol I, pp 423–430

Nairn JA (1997) Fracture mechanics of composites with residual thermal stresses. J Appl Mech 64:804–810

Nairn JA (1999) Applications of finite fracture mechanics for predicting fracture events in composites. In: Fifth Int'l Conf. on Deformation and Fracture of Composites, London, UK, March 18-19, 1999, pp 1–10

Nairn JA (2000) Comprehensive Composite Materials, vol 2, Elsevier Science, Ed. R. Talreja and J.-A. E. Månson, chap Matrix Microcracking in Composites, pp 403–432

Nairn JA (2007) A numerical study of the transverse modulus of wood as a function of grain orientation and properties. Holzforschung 61:406–413

Nairn JA (2010) Polar shear-lag analysis of a composite of concentric cylinders with longitudinal cracks: Application to internal checking in wood. Composites Part A: Applied Science and Manufacturing 41(7):850 – 858, DOI DOI: 10.1016/j.compositesa.2010.02.017, URL http://www.sciencedirect.com/science/article/B6TWN-4YH56GC-2/2/a2bab0a21976664588b6e14a613df4a7

Nairn JA (2017) Cross-laminated timber properties including effects of non-glued edges and additional cracks. European Journal of Wood and Wood Products 75(6):973–983

Nairn JA, Hu S (1992) The initiation and growth of delaminations induced by matrix microcracks in laminated composites. Int J Fract 57:1–24

Nairn JA, Hu S (1994) Damage Mechanics of Composite Materials, Elsevier, Amsterdam, Ed. Ramesh Talreja, chap Micromechanics of Damage: A Case Study of Matrix Microcracking, pp 187–243

Nairn JA, Kim SR (1992) A fracture mechanics analysis of multiple cracking in coatings. Engr Fract Mech 42:195–208

Nairn JA, Hu S, Bark JS (1993) A critical evaluation of theories for predicting microcracking in composite laminates. J Mat Sci 28:5099–5111

O'Brien TK (1984) Mixed-mode strain-energy-release rate effects on edge delamination of composites. Effects and Defects in Composite Materials ASTM STP 836:125–142

O'Brien TK (1985) Delamination and Debonding of Materials, vol STP 876, ASTM, Ed. W. S. Johnson, chap Analysis of Local Delaminations and Their Influence on Composite Behavior, pp 282–297

Oh JK, Lee JJ, Hong JP (2015) Prediction of compressive strength of cross-laminated timber panel. Journal of Wood Science 61(1):28–34

Pang S, Orchard R, McConchie D (1999) Tangential shrinkage of pinus radiata earlywood and latewood, and its implication for within-ring internal checking. New Zealand Journal of Forestry Science 29(3):484–491

Paris PC, Gomez RE, Anderson WE (1961) A rational analytical theory of fatigue. The Trend in Engineering 13:9–14

Parvizi A, Garrett KW, Bailey JE (1978) Constrained cracking in glass fiber-reinforced epoxy cross-ply laminates. J Mat Sci 13:195–201

Reiterer A, Stanzl-Tschegg S, Tschegg E (2000) Mode I fracture and acoustic emission of softwood and hardwood. Wood Science and Technology 34(5):417–430

Salpekar SA, O'Brien TK (1991) Analysis of matrix cracking and local delamination in (0/θ/-θ)s graphite epoxy laminates under tension load. Proc 8^{th} Int'l Conf on Comp Mat Honolul, HI, USA, 28-G:1–14

Schniewind AP, Centeno JC (1973) Fracture toughness and duration of load factor I. six principal systems of crack propagation and the duration fractor for cracks propagating parallel to grain. Wood Fiber 5:152–159

Shir Mohammadi M, Nairn JA (2014) Crack propagation and fracture toughness of solid balsa used for cores of sandwich composites. Journal of Sandwich Structures and Materials 16(1):22–41

Williams JG (1984) Fracture Mechanics of Polymers. John Wiley & Sons, New York

Wilson E, Shir Mohammadi M, Nairn JA (2013) Crack propagation fracture toughness of several wood species. Advances in Civil Engineering Materials 2(1):316–327

Zabel RA, Morrell JJ (2012) Wood microbiology: decay and its prevention. Academic press